



**Pressure-Driven Chemical Lock-in Structure and Optical Properties in Sillen Compounds  $\text{PbBiO}_2\text{X}$  ( $\text{X} = \text{Cl}, \text{Br}, \text{and I}$ )**

Journal:	<i>Journal of Materials Chemistry A</i>
Manuscript ID	TA-ART-03-2020-003291.R1
Article Type:	Paper
Date Submitted by the Author:	29-May-2020
Complete List of Authors:	Zhang, Qian; Center for High Pressure Science and Technology Advanced Research (HPSTAR) Liu, Xuqiang; HPSTAR Li, Nana; Center for High Pressure Science and Technology Advanced Research, HPSTAR Wang, Bihan; Center for High Pressure Science and Technology Advanced Research (HPSTAR), Shanghai 201203, China Huang, Quan; Zhongyuan University of Technology, College of Material and Chemical Engineering Wang, Lin; Center for High Pressure Science & Technology Advanced Research , Zhang, Dongzhou; University of Hawaii Manoa, Hawaii Institute of Geophysics & Planetology Wang, Yonggang; Center for High Pressure Science & Technology Advanced Research, ; Yang, Wenge; Center for High Pressure Science and Technology Advanced Research,

1 Pressure-Driven Chemical Lock-in Structure and Optical Properties in  
2 *Sillen* Compounds  $\text{PbBiO}_2X$  ( $X = \text{Cl}, \text{Br}, \text{and I}$ )

3 Qian Zhang,<sup>†</sup> Xuqiang Liu,<sup>†</sup> Nana Li,<sup>†</sup> Bihan Wang,<sup>†</sup> Quan Huang,<sup>‡</sup> Lin Wang,<sup>†</sup> Dongzhou Zhang,<sup>£</sup>  
4 Yonggang Wang,<sup>†,\*</sup> and Wenge Yang<sup>†,\*</sup>

5 <sup>†</sup>Center for High Pressure Science and Technology Advanced Research (HPSTAR), Shanghai 201203,  
6 China.

7 <sup>‡</sup>College of Material and Chemical Engineering, Zhongyuan University of Technology, Zhengzhou  
8 450007, China

9 <sup>£</sup>Hawaii Institute of Geophysics & Planetology, University of Hawaii Manoa, Honolulu, Hawaii 96822,  
10 USA

11

## 1 ABSTRACT

2 *Sillen* compounds with general formula  $\text{PbBiO}_2\text{X}$  ( $\text{X} = \text{Cl}, \text{Br}, \text{I}$ ) are frequently studied as photocatalysts,  
3 and have attracted widespread attention due to their degradation of organic contaminants and water  
4 oxidation under visible light irradiation. Among many photoelectric materials, the band gap has been  
5 reduced approaching to the optimum value by pressure (1.34 eV for photovoltaic materials according  
6 to the Shockley–Queisser limit), which is favorable to their photo-responsive applications. However,  
7 such enhanced properties are usually restored after the pressure is released. Here, by combing the  
8 pressure and chemical engineering tools together, we discovered that by selecting appropriate elemental  
9 species, the optimized structure and optical band gap of  $\text{PbBiO}_2\text{Br}$  can be locked after compression-  
10 decompression treatment cycling. The pressure-induced strain retention in  $\text{PbBiO}_2\text{Br}$  could be the cause  
11 of the structural and optical irreversible behavior. Moreover, compression behavior and optical band  
12 gap under high pressure in  $\text{PbBiO}_2\text{X}$  system were studied systematically by in-situ high pressure  
13 synchrotron X-ray diffraction, UV-Vis absorption spectroscopy and resistivity experiments. Along with  
14 the enhanced photocurrent under compression,  $\text{PbBiO}_2\text{X}$  compounds under external pressure exhibit  
15 great potential for photocatalytic applications under solar light irradiation. In a suitable element  
16 category, the pressure driven structural lock-in preserves its optical performance, opening up a new  
17 window for manipulating and filtrating better multifunctional materials.

18

19

20

## 1 INTRODUCTION

2 Mixed-anion compound beyond one anionic species in a single phase offers an opportunity to design and  
3 control novel physical and chemical properties due to the flexibility of its semiconductor structure and  
4 composition.<sup>1</sup> Especially, bismuth-containing semiconductors afford many potential applications in  
5 thermoelectric,<sup>2-5</sup> ferroelectrics<sup>6-9</sup> and photocatalytic fields,<sup>10-18</sup> owing to the stereoactive  $6s^2$   
6 configuration of Bi, as well as the modulated crystal/electronic structure by mixed anions with distinct  
7 electronegativity. For example, the oxyselenide BiCuSeO crystallizes in a regular stack of conductive  
8  $[\text{Cu}_2\text{Se}_2]$  sheets and insulating  $[\text{Bi}_2\text{O}_2]$  sheets. In favor of its layered structure, the intrinsic low thermal  
9 conductivity ( $0.60 \text{ Wm}^{-1}\text{K}^{-1}$  at room temperature) and the narrow band gap ( $\sim 0.8 \text{ eV}$ ) makes it a promising  
10 candidate for the high efficient thermoelectric application.<sup>4, 5</sup> It is found that some Bi-based oxyhalide  
11 Aurivillius compounds also adopt an intergrowth of fluorite-like  $[\text{Bi}_2\text{O}_2]$  and perovskite-like  $[\text{A}_{n-1}\text{B}_n\text{O}_{3n+1}]$   
12 units, such as  $\text{Bi}_4\text{NbO}_8\text{Cl}$ ,  $\text{Bi}_4\text{TaO}_8\text{Cl}$ , and  $\text{Bi}_3\text{Pb}_2\text{Nb}_2\text{O}_{11}\text{Cl}$ . Their ferroelectricity was widely studied,  
13 owing to their polar structure, although the neutron diffraction revealed that a ferroelectric-type phase  
14 transition occurred at high temperature from an ideal tetragonal to orthorhombic or pseudo-tetragonal  
15 structure.<sup>8, 9</sup> In addition, some other closely related layered oxyhalides, such as the *sillen* family, exhibit  
16 excellent photocatalytic properties.<sup>18</sup> Under solar light irradiation, they were reported to achieve the  
17 organic pollutant decomposition,<sup>14, 15</sup> wastewater purification, and water oxidation.<sup>17, 19</sup> So far, the  
18 chemical strategies for approaching better performance on layered Bi-based semiconductors are primarily  
19 dedicated to the composition and morphology engineering, all of which are subjected to the fabrication  
20 process.

21 Pressure, as an alternative approach to modify physical/chemical properties in modern material science,  
22 has been proven as a clean efficient route to tune the crystal structure and electronic configuration for  
23 photoelectric materials.<sup>20-22</sup> Recently, it has been reported that with applied external pressure, bismuth

1 oxyhalides BiOCl suffered from a redistribution of Bader charge among its component ions. A following  
2 isostructural phase transition was noticed experimentally, as proved by abnormal lattice compression ( $c/a$ )  
3 within the pressure range from 15.1 GPa to 22.1 GPa.<sup>23</sup> Our previous pressure response studies on bismuth  
4 oxychalcogenides have also demonstrated a steady anisotropic lattice contraction upon compression. Due  
5 to the pressure-induced competition between charge delocalization and band gap opening, the electrical  
6 resistivity rollback was observed beyond 12 GPa.<sup>24</sup> All these findings encourage us to gain deep insight  
7 into the structure-properties relationship for other Bi-based mixed anion compounds under high pressure,  
8 which has been rarely reported so far.

9 *Sillen X* compounds are typical layered semiconductors with single/multiple layers of *X* atom  
10 intercalated in between the fluorite-like Bi<sub>2</sub>O<sub>2</sub>-based layers.<sup>25, 26</sup> With single halogen atom layer insertion,  
11 PbBiO<sub>2</sub>X ( $X=Cl, Br, I$ ) exhibits potential visible-light-responsive photocatalytic activities in water  
12 oxidation or degradation of organic pollutants due to their appropriate band levels.<sup>17, 27</sup> In this work, by  
13 selecting series X species ( $X=Cl, Br, I$ ), we conducted the in-situ comparison studies on structure and  
14 optical property under high pressure with synchrotron x-ray diffraction and optical absorption methods,  
15 and for the first time, discovered the band-gap narrowing for all of them during compression, but only  
16 PbBiO<sub>2</sub>Br retained partially high pressure structure and property upon decompression. The narrowed  
17 band-gap for the pressurized PbBiO<sub>2</sub>Br get closer to the pristine PbBiO<sub>2</sub>I, which has the narrowest band-  
18 gap among these three compounds. From our results, external pressure could be used as a great potential  
19 tool towards better semiconducting materials with engineered band gaps through irreversible pressure-  
20 induced phase transformation. The abnormal structural, optical and transport behaviors of PbBiO<sub>2</sub>X could  
21 be achieved by combining the chemical and pressure efforts together.

## 22 EXPERIMENTAL DETAILS

1 **Sample syntheses.** As the precursor to synthesize the target  $\text{PbBiO}_2X$  ( $X = \text{Cl}, \text{Br}, \text{and I}$ ) samples via a  
2 two-step procedure, the particulate  $\text{BiOX}$  reactants were initially prepared by a co-precipitation method  
3 as follows:  $\text{Bi}(\text{NO}_3)_3 \cdot 5\text{H}_2\text{O}$  (Aladdin, 99.0%) was added slowly into solution containing stoichiometric  
4 amounts of  $\text{NaCl}$  (Rhawn, 99.5%),  $\text{NaBr}$  (Rhawn, 99.5%), and  $\text{KI}$  (Rhawn, 98.5%) respectively, with the  
5  $\text{Bi}:X$  molar ratio of 1:1. The mixture was stirred at room temperature for 0.5 hour in air and washed with  
6 distilled water and ethanol, followed by drying at  $60^\circ\text{C}$  for 10 hours. During the process of  $\text{PbBiO}_2X$ , the  
7 well-mixed powders of  $\text{BiOX}$  and  $\text{PbO}$  (Aladdin, 99.5%) with the stoichiometric proportion were calcined  
8 at  $700^\circ\text{C}$  for 24 hours in alumina crucibles. The phase identification of the obtained products was carried  
9 out on an XPert Powder (analytical) X-Ray diffractometer (XRD) with  $\text{Cu } K\alpha$  radiation.

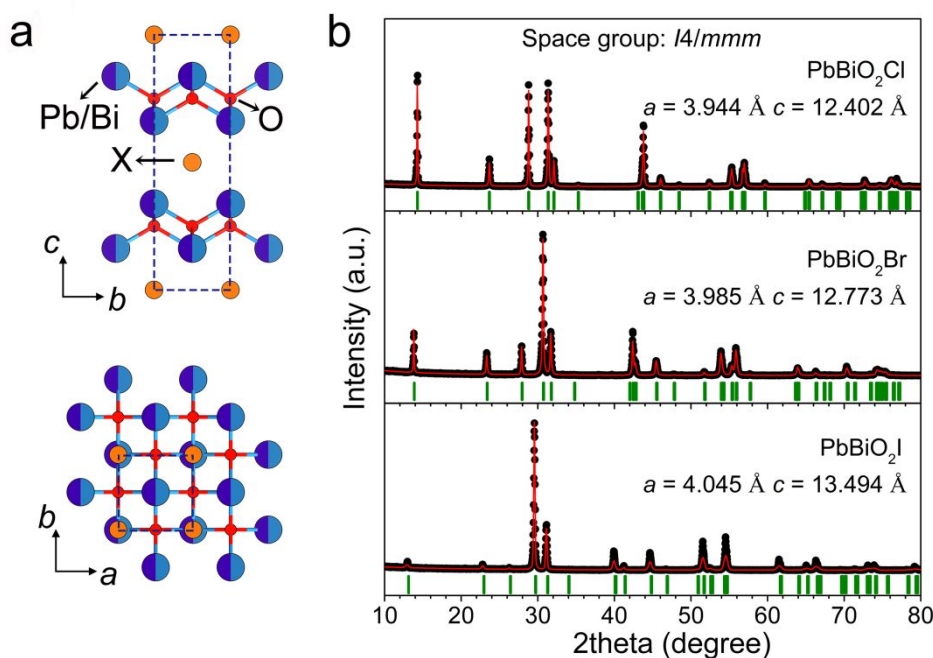
10 **High pressure characterizations.** Symmetrical diamond anvil cells (DAC) with  $300\ \mu\text{m}$  culet-size anvils  
11 were employed in all high pressure experiments, which could facilely generate pressure beyond 50 GPa.  
12 T301 stainless steel foils were pre-indented to  $50\ \mu\text{m}$  in thickness, where cavities were drilled by infrared  
13 laser with  $150\ \mu\text{m}$ -diameter. All fine-grinding powders were pressed into pellets with about  $10\ \mu\text{m}$  in  
14 thickness and then loaded into above cavities together with small ruby balls. In this way, ruby was used  
15 to calibrate the pressure by the luminescence method. Silicone oil was added in the cavities to serve as  
16 the pressure-transmitting medium to provide a quasi-hydrostatic pressure environment. The in-situ high  
17 pressure angle-dispersive XRD experiments were carried out at 13 BM-C station of GSECARS at the  
18 Advanced Phonon Source (APS), in Argonne National Laboratory (ANL). A monochromatic X-ray beam  
19 ( $\lambda = 0.4340\ \text{\AA}$ ) was focused to  $15\ \mu\text{m}$  in diameter (FWHM) in our diffraction experiments.<sup>28</sup> Two-  
20 dimensional diffraction patterns were recorded on a charge-coupled device (CCD) detector. The  $\text{LaB}_6$   
21 standard powder was used to calibrate the distance between sample and detector and the orientation  
22 parameters of the detector. The diffraction patterns were integrated using the program Dioptas.<sup>29</sup> It is  
23 worth noting that the silicone oil can provide reasonable quasi-hydrostatic pressure environment below

1 15 GPa, which may introduce the pressure gradient inside the sample chamber, especially at high pressure  
2 region. Typically the pressure variation is less than 0.2 GPa and no more than 0.5 GPa above 15 GPa. The  
3 crystal structures were refined with Rietveld method by using the General Structure Analysis System  
4 (GSAS) program packages.<sup>30</sup> In-situ high-pressure optical measurements were performed on an UV-Vis  
5 absorption spectrophotometer with the acquisition time of 2 s at room temperature (RT). Each reference  
6 was collected on the sample-free area with the same grating size and exposure time. The optical band gap  
7 was determined from Tauc plot, a linear dependence for  $(\alpha dh\nu)^2$  versus energy  $h\nu$ , where  $\alpha$  is the  
8 absorption coefficient,  $d$  is the sample thickness,  $h$  and  $\nu$  are Planck's constant and frequency,  
9 respectively. The resistance measurements under high pressure were carried out by using the four-probe  
10 method, which was described in detail previously.<sup>24</sup> The resistivity was calculated by the Van de Pauw  
11 equation.<sup>31</sup> For the photocurrent measurements, a Zahner IM6 electrochemical workstation was utilized  
12 to record the I-t data by applying a constant bias voltage of 1 V. A 500 W Xeon lamp was utilized as the  
13 irradiation source ( $\sim 5 \text{ mWcm}^{-2}$  on the sample). The photo response measurements were monitored in the  
14 dark and under illumination in DAC devices.

## 15 RESULTS AND DISCUSSION

16 **Syntheses and crystal structures of  $\text{PbBiO}_2\text{X}$ .** As typical *Sillen X* compounds, they are composed of  
17 single halide anions [X] slab sandwiched by two-dimensional (2D) edge-shared  $\text{O}(\text{Bi}/\text{M})_4$  tetrahedra  
18 units.<sup>26</sup> The introduction of aliovalent cations offers even broader opportunities for original structural  
19 topologies based on  $\text{OBi}_4$  units.  $\text{CaBiO}_2\text{Cl}$ ,  $\text{SrBiO}_2\text{X}$  and  $\text{BaBiO}_2\text{X}$  adopted a monoclinic ( $P2_1/m$ ) and an  
20 orthorhombic ( $Cmcm$ ) unit cells, where Bi is partially replaced by alkaline earth metal.<sup>11</sup> Here Bi is  
21 partially replaced by Pb with the same stereoactive  $6s^2$  lone pair configuration.<sup>25</sup> The naturally mineral  
22 perite  $\text{PbBiO}_2\text{Cl}$  were reported to crystallize in the orthorhombic structure. However, our XRD  
23 examinations show three profiles of  $\text{PbBiO}_2\text{X}$  match well with the standard powder diffraction files

1 (PDF#39-0802, PDF#38-1008, PDF#78-0521) with same tetragonal symmetry  $I4/mmm$ , as shown in Fig.  
 2 1. As the ionic size increases from Cl to I, both lattice  $a$  and  $c$  are expanded,  $c/a$  ratio increase, since the  
 3 X ion layers are intercalated between  $(\text{Bi/Pb})_2\text{O}_2$  layers without changing these layers. The refined lattice  
 4 parameters are:  $a = 3.944 \text{ \AA}$ ,  $c = 12.402 \text{ \AA}$  for chloride,  $a = 3.985 \text{ \AA}$ ,  $c = 12.773 \text{ \AA}$  for Bromide, and  $a =$   
 5  $4.045 \text{ \AA}$ ,  $c = 13.494 \text{ \AA}$  for Iodide, respectively. Tiny deviations less than 0.2% agree well with Ketterer et  
 6 al.'s report on them.<sup>25</sup>

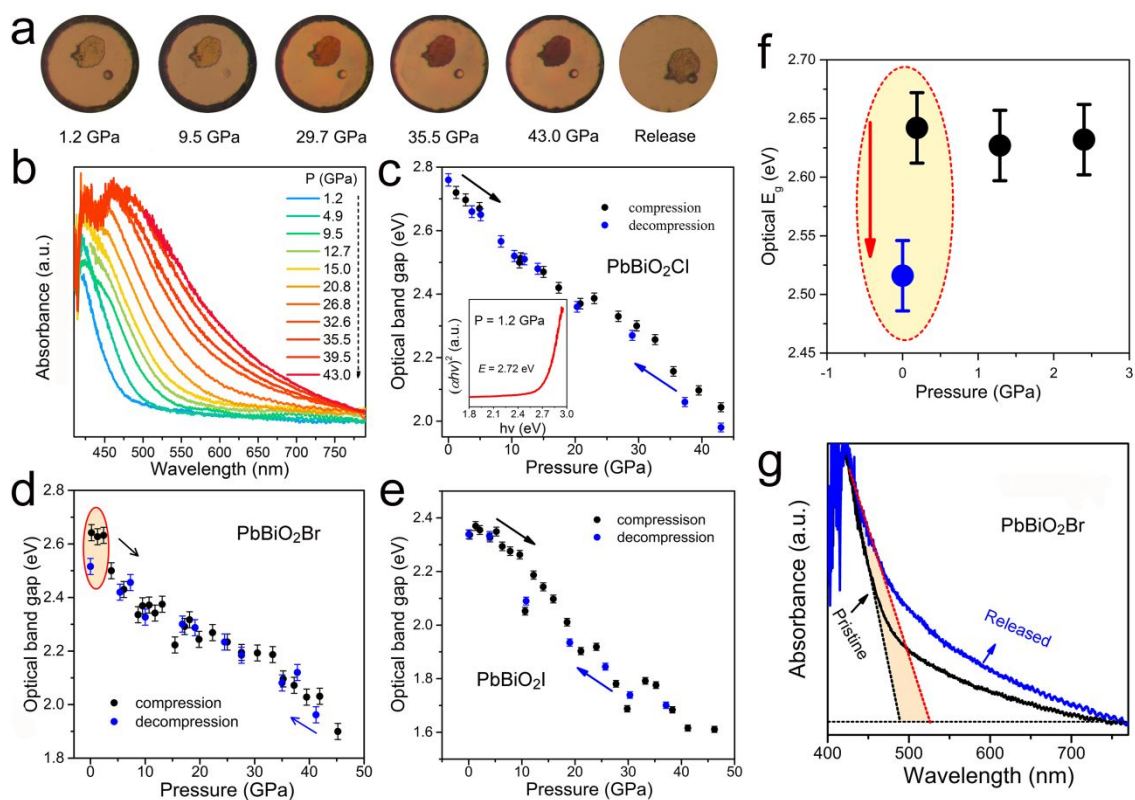


7  
 8 **Fig. 1.** Crystal structures of  $\text{PbBiO}_2\text{X}$  ( $X = \text{Cl}, \text{Br}, \text{I}$ ). (a) The tetragonal structure viewed along  $[100]$  and  
 9  $[001]$ . (b) Rietveld refinement results of the  $\text{PbBiO}_2\text{X}$  samples with space group  $I4/mmm$ . In (b),  
 10 experimental: black circle; simulation: red lines; Bragg reflections: olive bars.

11 **Reversible/irreversible optical property evolutions.** Hydrostatic pressure can greatly affect the  
 12 physical/chemical properties of functional materials, including the band gap adjustment. In order to track  
 13 the optical behavior response to the external pressure, we performed the UV-Vis absorption measurements  
 14 on  $\text{PbBiO}_2\text{X}$  at various pressures. At ambient pressure,  $\text{PbBiO}_2\text{X}$  display steep absorption edges at about  
 15 517 nm, 538 nm and 563 nm (Fig. S1) from  $X = \text{Cl}, \text{Br}$  and  $\text{I}$ , respectively, which are consistent with



1 previous studies.<sup>12, 14, 17, 27</sup> As the pressure increases, we noticed a piezochromic transformation for  
2 chloride from a translucent yellow to dark red, and eventually opaque red at 43 GPa (Fig. 2a).  
3 Accordingly, the absorption edges of all samples maintained gradually redshift throughout the  
4 compression process. The slope of absorbance at the edge tends to gentle, which could be associated with  
5 the evolution of band structure, likely, a transformation from direct to indirect band gap. Meanwhile, over  
6 the entire visible range, the absorption increases with increasing pressure. Tauc plot analysis by  
7 extrapolating the linear portion of the  $(\alpha dh\nu)^2$  versus energy  $h\nu$  plot indicated a direct band gap of 2.76  
8 eV, 2.64 eV and 2.34 eV from  $X = \text{Cl, Br, I}$  at initial pressure point, as shown in Fig. 2c-e. Upon  
9 compression, the band gap suffered continuously reduction to 1.98 eV, 1.70 eV and 1.40 eV for  $\text{PbBiO}_2\text{Cl}$ ,  
10  $\text{PbBiO}_2\text{Br}$ , and  $\text{PbBiO}_2\text{I}$  at the maximum pressure of about 43 GPa. The narrowed band gaps can be  
11 explained by the pressure-enhanced orbital coupling of  $\text{Pb/Bi-6s}$  and  $X-np$ . Compared with the band gap  
12 tuning range of 0.42 eV (from 2.76 eV to 2.34 eV) with chemical replacement of X from Cl to I, the  
13 pressure effect is more significant to  $\sim 1$  eV ( $\text{PbBiO}_2\text{Cl}$ : 2.76-1.98 eV,  $\text{PbBiO}_2\text{Br}$ : 2.64-1.70 eV,  $\text{PbBiO}_2\text{I}$ :  
14 2.34-1.40 eV ) over 43 GPa for each X species. This finding is also realized in other layered bismuth  
15 oxychalcogenides.<sup>24, 32, 33</sup> Upon decompression, color of  $\text{PbBiO}_2\text{Cl}$  returns to the original translucent  
16 yellow, and the absorption edge completely recovers. The more exotic fact is, after releasing pressure,  
17 unlike chloride and iodide, bromide exhibits a partially retainable band gap of  $\sim 2.52$  eV, which is  $\sim 4.5\%$   
18 less than that of the starting  $\text{PbBiO}_2\text{Br}$  (Fig. 2f, g). The narrow band gap helps to absorb solar energy  
19 more widely. As vital photo-response parameters, both absorption enhancement and band gap narrowing  
20 could harvest solar light more effectively.



1

2 **Fig. 2.** (a) Optical microphotographs of PbBiO<sub>2</sub>Cl inside DAC during compression up to 43.0 GPa and  
 3 decompression, displaying piezochromic change from translucent yellow to dark red. (b-c) Optical  
 4 absorbance of PbBiO<sub>2</sub>Cl upon compression. The absorption edge redshifts with increasing pressure in  
 5 PbBiO<sub>2</sub>Cl. It recovered upon releasing pressure. The inset gives the direct bandgap Tauc plots of the  
 6 Kubelka-Munk function at 1.2 GPa for PbBiO<sub>2</sub>Cl. Magnitudes of band gaps can be estimated by  
 7 extrapolating the linear portion of the Tauc plots to the baselines. (d-e) Pressure dependence of optical  
 8 band gap of PbBiO<sub>2</sub>Br and PbBiO<sub>2</sub>I upon both compression and decompression. (f) The bandwidth before  
 9 and after compression for PbBiO<sub>2</sub>Br. (g) Comparison of the absorbance before and after pressure  
 10 treatment in PbBiO<sub>2</sub>Br. You should change the ambient in (g) to pristine because both measurements are  
 11 at ambient pressure.

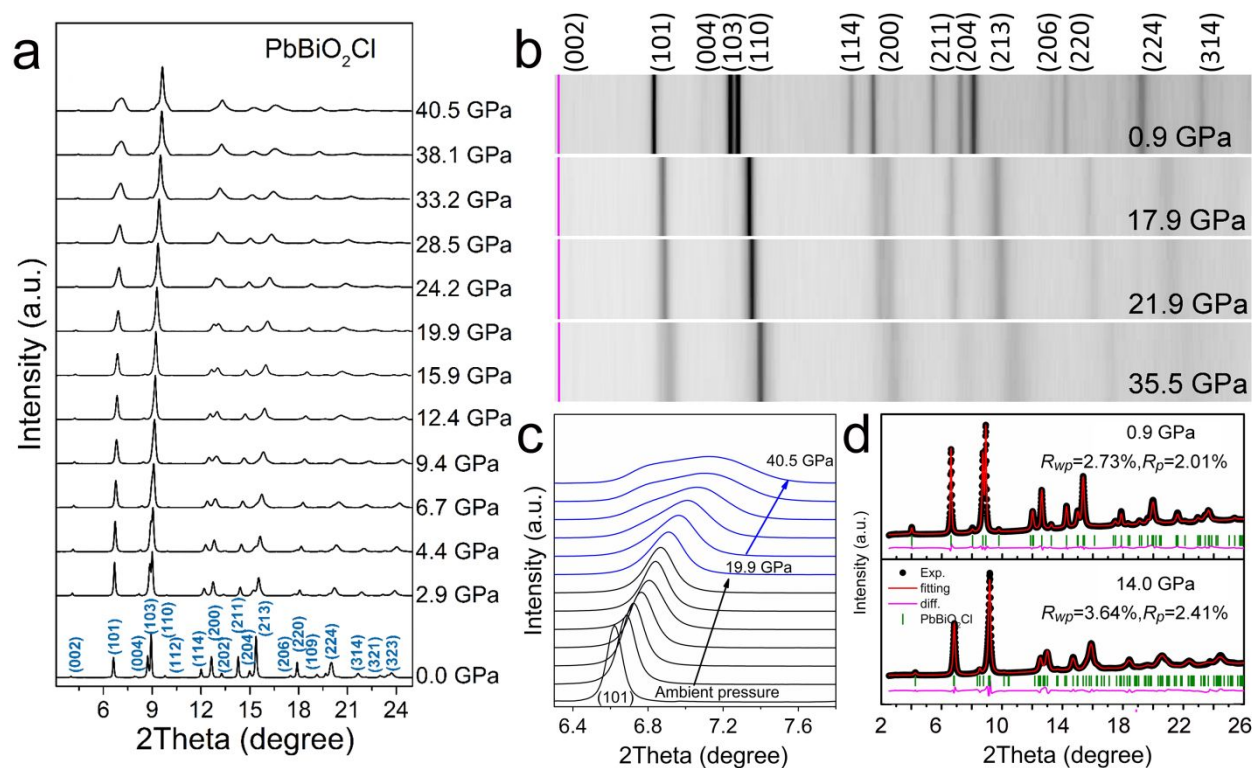
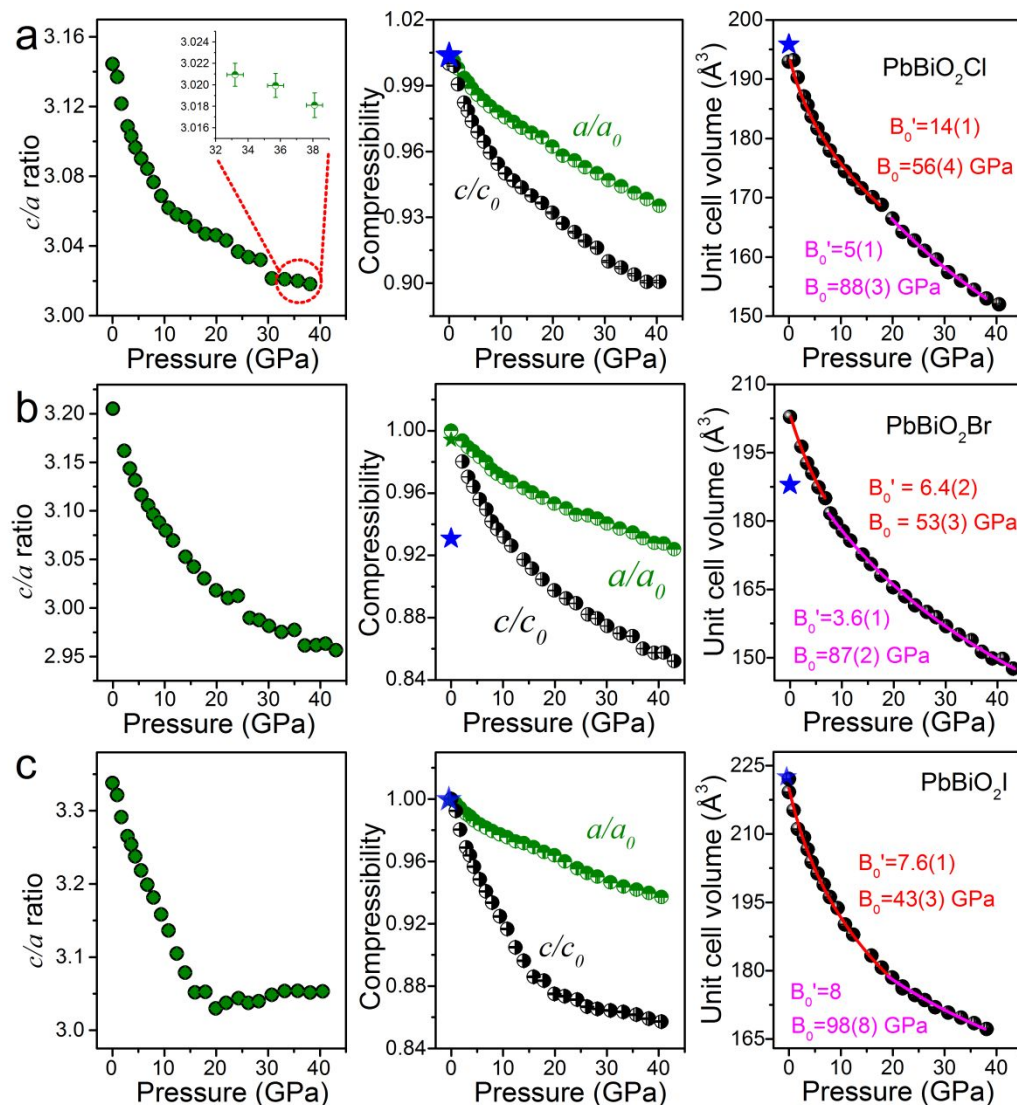


**Fig. 3.** Selected angle-dispersive XRD patterns of  $\text{PbBiO}_2\text{Cl}$  with incident  $\lambda = 0.4340 \text{ \AA}$  at RT (a). (b) 2D images of  $\text{PbBiO}_2\text{Cl}$  at 0.9 GPa, 17.9 GPa, 21.9 GPa and 35.5 GPa, respectively (c) The evolution of (101) reflections under pressure. (d) Two refinement results for  $\text{PbBiO}_2\text{Cl}$  at 0.9 GPa and 14 GPa.

The optical band gap evolution can be correlated with changes in the structure under pressure. Fig. 3a shows the typical synchrotron XRD patterns of  $\text{PbBiO}_2\text{Cl}$  at selected pressures. All sharp XRD peaks of the samples can be well indexed into the space group  $I4/mmm$ . As the pressure increases, all the reflections shift to higher  $2\theta$  angle, indicating lattice contraction with pressure. No noticeable extra peaks suggest the initial structure symmetry was retained at elevated pressure up to 40.5 GPa, the highest pressure applied. Similar structure evolution can also be found for  $\text{PbBiO}_2\text{Br}$  and  $\text{PbBiO}_2\text{I}$  in Fig. S2. Generally, the peak widths of XRD at high pressure increase, typically caused by non-hydrostatic stress and other factors involving grain size reduction and the increased local stain.<sup>34, 35</sup> However, the peaks (101) for  $\text{PbBiO}_2\text{Cl}$  centered at around  $6.62^\circ$  at ambient pressure broaden abnormally at high pressure, as shown in Fig. 3b. Careful cake two-dimension images display that the line width of (101) diffraction peak becomes

1 dissipation gradually with increasing pressure, rather than splitting (Fig. 3c). We deduce that symmetry  
 2 has not broken here. By using GSAS package to perform Rietveld refinement on  $\text{PbBiO}_2\text{X}$  with the same  
 3 tetragonal structure under high pressure, good agreement factors as shown in Fig. S3 can be obtained.



5 **Fig. 4.** Evolution of the lattice parameters  $c/a$ , the compressibility and unit cell volume of  $\text{PbBiO}_2\text{X}$  as a  
 6 function of pressure for: (a)  $\text{PbBiO}_2\text{Cl}$ , (b)  $\text{PbBiO}_2\text{Br}$ , and (c)  $\text{PbBiO}_2\text{I}$ . Red and pink lines are EoS fitting  
 7 results. Insets give the compressibility  $c/c_0$  and  $a/a_0$ . The error bars which comes from the Rietveld  
 8 refinement, are covered by the symbols. The enlarge view highlight the size of  $c/a$  error lines for  
 9  $\text{PbBiO}_2\text{Cl}$ .

1 The lattice parameters of  $\text{PbBiO}_2X$  based on Le Bail refinements method were plotted versus pressure  
 2 in Fig. 4. The  $c$  to  $a$  ratio ( $c/a$ ) decreased markedly with pressure first, and then shows a gentle variation  
 3 as further increasing pressure. Under pressure, compression of  $\text{PbBiO}_2X$  is anisotropic with the soft  
 4 direction along the  $c$  axis. Especially for  $\text{PbBiO}_2\text{I}$ , it reached a minimum ( $c/a$  dropped about 9.2% from  
 5 3.34 to 3.03) at 19.9 GPa. The abnormal relationship of  $c/a$  versus pressure for  $\text{PbBiO}_2\text{I}$  could distinctly  
 6 reflect the isostructural phase transition process, which has been proposed in many similar layered  
 7 compounds.<sup>36, 37</sup> The more pressure-sensitive  $c$  axis shrinkage results from the considerable interspaces  
 8 between  $(\text{Bi/Pb})_2\text{O}_2$  layer and single  $X$  atom layer. The rigid  $c$ -axis for high pressure phase mainly arises  
 9 from the stronger interlay  $\text{Pb}(\text{Bi})$ -iodine bonding. Lattice  $a$  collapse slightly at 17.9 GPa for chloride and  
 10 10.0 GPa for Bromide, in the inset, which we proposed an isostructural change. This mild lattice change  
 11 could be associated with the evolution of lone-pair electrons configuration of bismuth upon compression.  
 12 In  $\text{PbBiO}_2X$ , the  $\text{Bi/Pb-O}$  and  $\text{Bi/Pb-Bi/Pb}$  bonding distances were compressed with increasing pressure  
 13 as shown in Fig. S4, while the bonding angles  $\text{Bi/Pb-O-BiPb}$  in the tetrahedron were distorted from  $105.60$   
 14  $^\circ$  /  $117.52$   $^\circ$  to  $103.79$   $^\circ$  /  $121.54$   $^\circ$ , which leads the compression of the tetrahedral layer. With non-oxygen  
 15 anion from Cl to I, the  $(\text{Bi/Pb})_4\text{O}$  tetrahedron is away from regular tetrahedron which is attributed to effect  
 16 of halogen atoms with different ionic radius. Next, we fitted the  $V$ - $P$  curves of  $\text{PbBiO}_2X$  with two sections  
 17 over the entire pressure range by means of the third-order Birch–Murnaghan equation of state (EoS), as  
 18 follows

$$P = \frac{3}{2} B_0 \left[ \left( \frac{V_0}{V} \right)^{2/3} - \left( \frac{V_0}{V} \right)^{5/3} \right] \times \left\{ 1 + \frac{3}{4} (B_0' - 4) \times \left[ \left( \frac{V_0}{V} \right)^{2/3} - 1 \right] \right\}$$

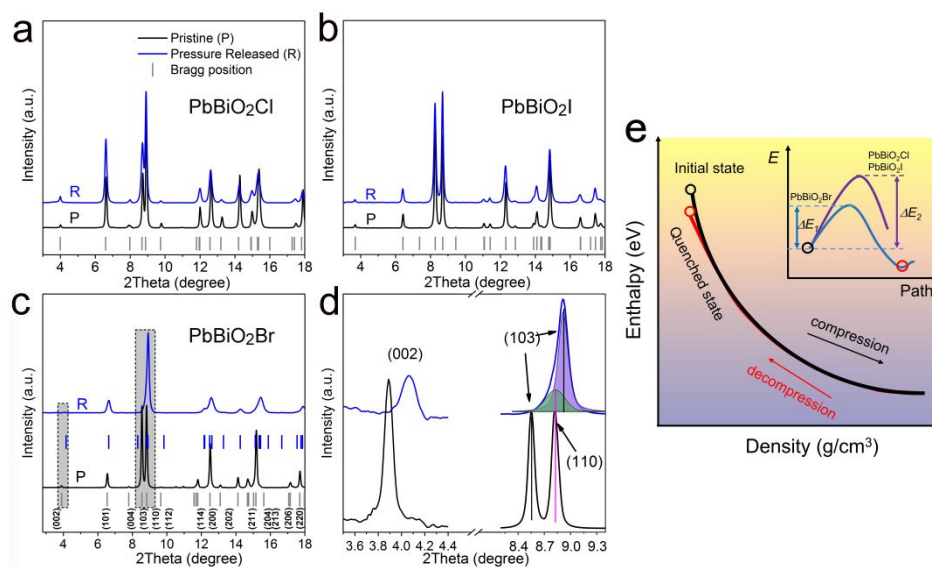
19 derivative of the bulk modulus with respect to pressure.<sup>38</sup> The isothermal bulk moduli  $B_0$  are yield to be  
 20 56(4) GPa, 53(3) GPa, and 43(3) GPa in the first pressure range for  $X = \text{Cl}$ ,  $\text{Br}$ , and  $\text{I}$ , respectively. The  
 21 reduced bulk module from chloride to iodide corresponds to an enhanced compressibility and decrease of  
 22 elastic stiffness as anions changing from Cl to I. In the higher pressure range,  $B_0$  is fitted as 88(3), 87(2),  
 23 98(8) GPa, which are much higher bulk moduli (about 60% higher) than those of low pressure phase.

1 In Bi-based sillen compounds, the lone pairs electrons the lone pair electrons play an important role on  
2 their photocatalysis application. The interaction between O-2p and Bi-6s can elevate O2p orbitals,  
3 favoring the redox reaction in Bi-based photocatalyst.<sup>39</sup> The phenomenone follows well the revised lone  
4 pair model proposed by Payne et al<sup>40</sup> and Walsh et al<sup>41</sup>. Most photocatalysis researches show the fact that  
5 lone pairs from post-transition metal cations (e.g., Sn<sup>2+</sup>, Sb<sup>3+</sup>, Pb<sup>2+</sup>, and Bi<sup>3+</sup>) may improve the visible  
6 light-responsive photocatalysis efficiency in water splitting applications.<sup>17</sup> Under high pressure, Cheng et  
7 al. found perovskite PbCrO<sub>3</sub> underwent an IPT at around 1.6 GPa, accompanying an insulator-metal  
8 transition. Based on the XANES measurements, they proposed that Pb 6s, 6p electrons are hybridized  
9 with Cr cations at low pressure phase, but after the phase transition, the 6s electrons of Pb restore to lone  
10 pair state, which causes the insulating to metallic transport property change.<sup>42</sup> Here, we also observed the  
11 IPT in PbBiO<sub>2</sub>X and presume it associated with the pressure-driven lone pair electrons configuration  
12 evolution. However, there is no conclusive evidence on the effect of Bi's lone pair on the compression  
13 behavior. It is indeed intriguing to clarify the role of the lone pair on the structure and properties at high  
14 pressure. A continuous development maybe required.

### 15 **Reversible/irreversible structural phase transition.**

16 XRD patterns before and after compression-decompression cycle of PbBiO<sub>2</sub>X were then compared in Fig.  
17 5a-c. The chloride and iodide analogs show good reversibility after pressure releasing. Surprisingly, the  
18 crystal structure of pressure-released PbBiO<sub>2</sub>Br exhibits a partial retainable behavior. The XRD peaks  
19 from pressure-released PbBiO<sub>2</sub>Br (even after 12 hours relaxation) shifted to larger  $2\theta$  range than the  
20 pristine sample. In Fig. 5d, the enlarged XRD profiles from the hatched regions in Fig. 5c show clear  
21 differences between pristine and pressure-released PbBiO<sub>2</sub>Br samples. The (002) peak shifted to higher  
22  $2\theta$  angle along with the (110) and (103) peak merging for the decompressed PbBiO<sub>2</sub>Br. By distinguishing  
23 them via peak fitting, it can be seen that the (103) peak shifts to higher  $2\theta$  angle, while (110) almost

1 completely recovers, meaning the lattice constant  $c$  is largely not recovered due to the irreversible  
 2 interlayer compression. The unit cell parameters for pressure-released  $\text{PbBiO}_2\text{Br}$   $a = 3.965(2) \text{ \AA}$ ,  $c =$   
 3  $11.863(3) \text{ \AA}$ , and  $V = 187.9(3) \text{ \AA}^3$  are smaller than the initial values ( $a = 3.988(2) \text{ \AA}$ ,  $c = 12.774(3) \text{ \AA}$ , and  
 4  $V = 203.2(4) \text{ \AA}^3$ ). This drastically reduced  $c$  (7.1%), coupled with an almost total recovered  $a$ -lattice (0.6%  
 5 contraction), results in a volume reduction of 7.3%. The partial preserved crystal lattice could perfectly  
 6 explain the abovementioned retainable optical band gap for  $\text{PbBiO}_2\text{Br}$ .



7  
 8 **Fig. 5.** (a-c) XRD comparison before and after high pressure treatment up to 43 GPa for  $\text{PbBiO}_2\text{Cl}$ ,  
 9  $\text{PbBiO}_2\text{Br}$  and  $\text{PbBiO}_2\text{I}$ , respectively. P and R represent the pristine and after pressure released samples.  
 10 (d) Enlarged Bragg diffraction peaks (002), (103) and (110) from the hatched regions of Fig. 5(b). The  
 11 broad peak around  $8.9^\circ$  after pressure releasing is fitted with two individual peaks. (e) The hypothesis  
 12 enthalpy changes are driven by compression for  $\text{PbBiO}_2\text{X}$ . The reasonable small enthalpy difference  $\Delta E_1$   
 13 ( $\Delta E_1 > \Delta E_2$ ) between the ground state and quenched state for  $\text{PbBiO}_2\text{Br}$  leading to its retention structure  
 14 and properties.

15 As an alternative approach, pressure can provide energy and tune samples away from its ground state,  
 16 which allows the system to reach a metastable state with superior properties that could be preserved. Here,

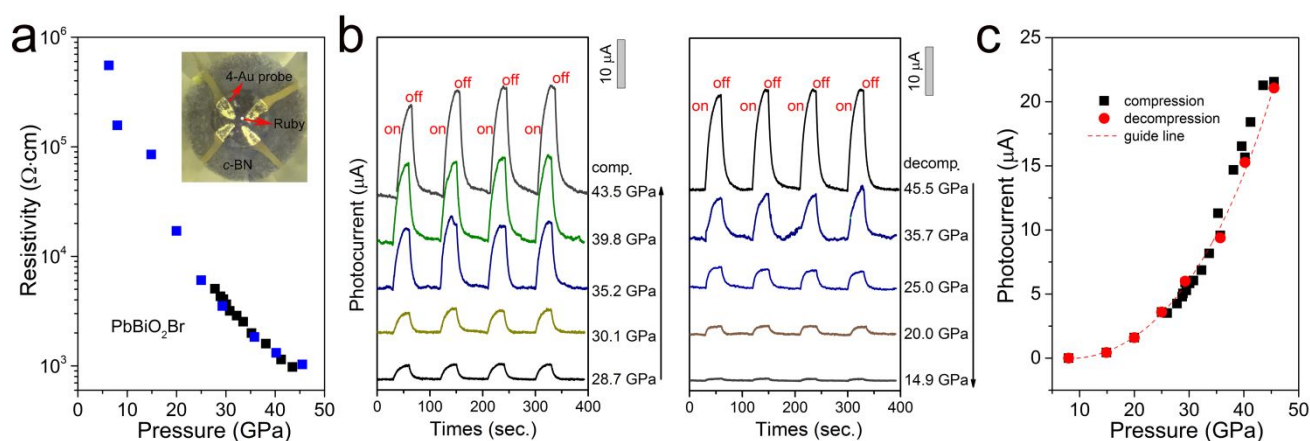


1 we plot a hypothesis thermodynamic diagram of enthalpy for  $\text{PbBiO}_2X$  in Fig. 5e. The black and red  
2 curves represent the compression and decompression enthalpy change as a function of pressure,  
3 respectively. The quenched state (red circle) is more energetically favored when the unit cell is more  
4 compressed comparing to the initial state (black circle). From a thermodynamic point of view, the  
5 magnitude of energy barrier depends on the detail path of the structure transition. Liu et al.<sup>43</sup> has reported  
6 the preserved structures and properties from high pressure treatment in hybrid perovskite  $(\text{BA})_2(\text{MA})\text{Pb}_2\text{I}_7$ ,  
7 in which the Pb-I-Pb angle is closer to  $180^\circ$  after compression and decompression process comparing to  
8 the as-prepared sample, which enables a better mixture of the Pb s and I p orbitals. *c*-axis in the quenched  
9  $\text{PbBiO}_2\text{Br}$  is smaller than that in the pristine material, which means the interlayer distance along *c*-axis is  
10 not totally recovered after fully release, enabling a strong hybridization of Pb/Bi 6s-6p and X p orbitals.  
11 As a result, a narrower band gap and wider visible light absorbance have been achieved. Therefore, we  
12 believe with proper chemical atoms/ions pressure can be used as a practical tool to lock-in the structure  
13 and physical properties in materials.

14 **Transport properties and photocurrent.** In-situ high-pressure conductivity measurement was  
15 performed on  $\text{PbBiO}_2\text{Br}$  by using the quasi-four-probe methods within a DAC, to better understand the  
16 pressure-tailoring electronic properties. Fig. 6a shows the electrical resistivity evolution of  $\text{PbBiO}_2\text{Br}$  as  
17 a function of pressure upon compression and decompression. The initial high pressure was applied to  
18 ensure intimate contact between the powder sample and the Au contact leads. As the pressure increases,  
19 the resistivity drops quickly, up to almost 3 orders of magnitude at 45 GPa. Usually, pressure can enhance  
20 orbital overlapping and increase band dispersion, so the hybridization of Pb/Bi<sub>6s</sub> and O<sub>2p</sub> orbital could  
21 cause the monotonic decrease in resistivity.<sup>24, 32</sup> After decompression, the structure changes back to a low  
22 density state, leading to a reversible high resistance. Furthermore, as a reference, we also measured the  
23 resistance evolution of  $\text{PbBiO}_2\text{I}$ , which displays similar behavior to that for the Br-based analog (see Fig.



1 S5). The conductivities of  $\text{PbBiO}_2\text{X}$  improve significantly under extreme pressure, which may provide  
 2 some novel application prospects in photoelectrochemical devices.



4 **Fig. 6.** (a) Resistivity of  $\text{PbBiO}_2\text{Br}$  versus pressure during compression and decompression. Black and  
 5 blue solid symbols represent the compression and decompression procedures, respectively. (b) Pressure-  
 6 dependent transient photocurrent responses of  $\text{PbBiO}_2\text{Br}$  under a visible light illumination for several  
 7 light-on-off cycles. (c) Photocurrent  $I$  as a function of pressure during compression and decompression.

8 Another essential feature of photocatalytic with photoelectrochemical applications is photo  
 9 responsiveness. We evaluated the in-situ transient photocurrent response for  $\text{PbBiO}_2\text{Br}$  under the  
 10 simulated solar illumination. As shown in Fig. 6b and c,  $\text{PbBiO}_2\text{Br}$  exhibits a reproducible photocurrent  
 11 response under high pressure, which follows swiftly with the light on and off, demonstrating the visible  
 12 light activity and photochemical stability for our sample. The discernable photocurrent under high  
 13 pressure from 28.7 GPa up to 43 GPa indicated a semiconductor feature as a photovoltaic/photocatalytic  
 14 material. As the pressure increase, the photocurrent  $I_{\text{ph}}$  ( $I_{\text{ph}} = I_{\text{illuminated}} - I_{\text{dark}}$ ) was indiscernible at ambient  
 15 condition, and enhanced significantly to 21.5  $\mu\text{A}$  ( $\sim 48.6 \text{ mA}\cdot\text{cm}^{-2}$  for  $\sim 140 \text{ mW}\cdot\text{cm}^{-2}$  illumination) at  
 16 45.5 GPa. It is more than 4 orders of magnitude higher than the one reported at ambient pressure ( $\sim 1.2$   
 17  $\mu\text{A}\cdot\text{cm}^{-2}$ )<sup>27</sup>. This significantly enhanced photocurrent comes mainly from the remarkable enhancement in  
 18 conductivity. As discussed above, structural changes under high pressure inherit the layered structural

1 feature, which can explain the persistent photocurrent. As marked with the blue symbols and dashed line  
2 in Fig. 6d, the photocurrent reverted with decreasing pressure. In *sillen* systems, the pressure-induced  
3 switchable photo responsiveness may be closely related to the reversible structure and resistance, and  
4 indicates its potential photocatalysis and applications as a switcher or controller.

5 It is well-known that high-pressure research has made unprecedented progress in organic-inorganic  
6 halide perovskites by modifying the structure and properties, especially reducing the band gap toward  
7 more efficiency of harvesting solar energy for photovoltaic applications.<sup>35</sup> In this work, parallel band gap  
8 modulation has been successfully spread to complex bismuth-based semiconductors with a layered  
9 structure. More importantly, the pressure-induced structural and optical reversibility and irreversibility in  
10 *sillen* X compound demonstrates a framework for understanding in depth structure-property relationships  
11 of *sillen* compounds, and provides new dimension for the rational design of semiconductors with tailored  
12 applications in optoelectronic/photoelectrochemical units.

## 13 CONCLUSIONS

14 Pressure and chemical engineering tools were applied to the layered semiconductors  $\text{PbBiO}_2\text{X}$  ( $X = \text{Cl}$ ,  
15  $\text{Br}$ ,  $\text{I}$ ) in order to achieve better photoelectrochemical performance. Under compression, three  $\text{PbBiO}_2\text{X}$   
16 undergo a robust tetragonal structural evolution, and present an anisotropic compression behavior owing  
17 to their layered structural feature.  $\text{PbBiO}_2\text{X}$  exhibit continuously narrowed band gaps under compression,  
18 which could be associated with the pressure-induced Bi-O bond shortening, and the distortion within the  
19  $\text{PbBiO}_2$  layer. Intriguingly, both the crystal structures and the band gaps of  $\text{PbBiO}_2\text{Cl}$  and  $\text{PbBiO}_2\text{I}$  are  
20 recoverable after pressure releasing, while,  $\text{PbBiO}_2\text{Br}$  shows partially irreversible in both structural and  
21 optical properties. The probable mechanism of the irreversible behavior was also proposed, which was  
22 attributed to the unrecovered strains of bromide after pressure-treatment compared to chloride and iodide  
23 analogs. A remarkably narrowed (2.52 eV, 4.5% drop) band gap of  $\text{PbBiO}_2\text{Br}$  compared to the initial  
24 value at ambient conditions was obtained after pressure is removed. By comparison of these three  
25 compounds, with the proper atomic size, some structure and optical properties can be locked-in on

1 PbBiO<sub>2</sub>X through high pressure processing. These findings highlight the synergistic effect of pressure and  
2 chemical engineering in optimizing electronic and optical performance, providing new directions for  
3 further access to novel multifunctional materials.

#### 4 ASSOCIATED CONTENT

##### 5 **Supporting Information**

6 Diffuse reflectance spectra of PbBiO<sub>2</sub>X at ambient condition, XRD patterns of PbBiO<sub>2</sub>Br and PbBiO<sub>2</sub>I at  
7 different pressures, GSAS refinement results PbBiO<sub>2</sub>X, bonding distance and angle changes with  
8 pressure, pressure dependence of resistivity of PbBiO<sub>2</sub>I.

#### 9 AUTHOR INFORMATION

##### 10 **Corresponding Authors**

11 \* Email: [yangwg@hpstar.ac.cn](mailto:yangwg@hpstar.ac.cn) (Wenge Yang)

12 \* Email: [yonggang.wang@hpstar.ac.cn](mailto:yonggang.wang@hpstar.ac.cn) (Yonggang Wang)

##### 13 **Notes**

14 The authors declare no competing financial interest.

#### 15 ACKNOWLEDGMENT

16 This work was financially supported by the National Nature Science Foundation of China (Grant Nos.  
17 51527801, 51772184, U1930401) and Science Challenge Project No. TZ2016001. PX<sup>2</sup> program is  
18 supported by COMPRES under NSF Cooperative Agreement EAR-1661511. APS is supported by DOE-  
19 BES, under Contract No. DE-AC02-06CH11357. The authors are also indebted to Dr. H. Zhang, J. Liu,  
20 F. Zhang, H. Dong for their technique assistance with UV-Vis spectrum and XRD experiments.

#### 21 REFERENCES

- 1 1. H. Kageyama, K. Hayashi, K. Maeda, J. P. Attfield, Z. Hiroi, J. M. Rondinelli and K. R.  
2 Poepelmeier, *Nat. Commun.*, 2018, **9**, 772.
- 3 2. G.-K. Ren, S.-Y. Wang, Y.-C. Zhu, K. J. Ventura, X. Tan, W. Xu, Y.-H. Lin, J. Yang and C.-W.  
4 Nan, *Energy Environ. Sci.*, 2017, **10**, 1590-1599.
- 5 3. X. Tan, J.-I. Lan, G. Ren, Y. Liu, Y.-H. Lin and C.-W. Nan, *J. Am. Ceram. Soc.*, 2017, **100**, 1494-  
6 1501.
- 7 4. L.-D. Zhao, J. He, D. Berardan, Y. Lin, J.-F. Li, C.-W. Nan and N. Dragoe, *Energy Environ. Sci.*,  
8 2014, **7**, 2900.
- 9 5. H. Hiramatsu, H. Yanagi, T. Kamiya, K. Ueda, M. Hirano and H. Hosono, *Chem. Mater.*, 2008,  
10 **20**, 326-334.
- 11 6. A. M. Kusainova, W. Z. Zhou, J. T. S. Irvine and P. Lightfoot, *J. Solid State Chem.*, 2002, **166**,  
12 148-157.
- 13 7. S. Liu, P. E. R. Blanchard, M. Avdeev, B. J. Kennedy and C. D. Ling, *J. Solid State Chem.*, 2013,  
14 **205**, 165-170.
- 15 8. A. M. Kusainova, P. Lightfoot, W. Zhou, S. Y. Stefanovich, A. V. Mosunov and V. A. Dolgikh,  
16 *Chem. Mater.*, 2001, **13**, 4731-4737.
- 17 9. A. M. Kusainova, S. Y. Stefanovich, V. A. Dolgikh, A. V. Mosunov, C. H. Hervoches and P.  
18 Lightfoot, *J. Mater. Chem.*, 2001, **11**, 1141-1145.
- 19 10. H. Kunioku, M. Higashi, O. Tomita, M. Yabuuchi, D. Kato, H. Fujito, H. Kageyama and R. Abe,  
20 *J. Mater. Chem. A*, 2018, **6**, 3100-3107.
- 21 11. H. Huang, S. Wang, Y. Zhang and X. Han, *Mater. Res. Bull.*, 2015, **62**, 206-211.
- 22 12. Z. Shan, X. Lin, M. Liu, H. Ding and F. Huang, *Solid State Sci.*, 2009, **11**, 1163-1169.
- 23 13. H. Kunioku, A. Nakada, M. Higashi, O. Tomita, H. Kageyama and R. Abe, *Sustain. Energy Fuels*,  
24 2018, **2**, 1474-1480.
- 25 14. S. Földner, P. Pohla, H. Bartling, S. Dankesreiter, R. Stadler, M. Gruber, A. Pfitzner and B. König,  
26 *Green Chem.*, 2011, **13**, 640-643.

- 1 15. H. Cheng, B. Huang and Y. Dai, *Nanoscale*, 2014, **6**, 2009-2026.
- 2 16. L. Ye, Y. Su, X. Jin, H. Xie and C. Zhang, *Environ. Sci. Nano.*, 2014, **1**, 90-112.
- 3 17. H. Suzuki, H. Kunioku, M. Higashi, O. Tomita, D. Kato, H. Kageyama and R. Abe, *Chem. Mater.*,
- 4 2018, **30**, 5862-5869.
- 5 18. J. Olchowka, H. Kabbour, M. Colmont, M. Adlung, C. Wickleder and O. Mentre, *Inorg. Chem.*,
- 6 2016, **55**, 7582-7592.
- 7 19. H. Fujito, H. Kunioku, D. Kato, H. Suzuki, M. Higashi, H. Kageyama and R. Abe, *J. Am. Chem.*
- 8 *Soc.*, 2016, **138**, 2082-2085.
- 9 20. W. L. Mao, H.-k. Mao, P. J. Eng, T. P. Trainor, M. Newville, C.-c. Kao, D. L. Heinz, J. Shu, Y.
- 10 Meng and R. J. Hemley, *Science*, 2003, **302**, 425-427.
- 11 21. Y. Ma, M. Eremets, A. R. Oganov, Y. Xie, I. Trojan, S. Medvedev, A. O. Lyakhov, M. Valle and
- 12 V. Prakapenka, *Nature*, 2009, **458**, 182-185.
- 13 22. A. Jaffe, Y. Lin, W. L. Mao and H. I. Karunadasa, *J. Am. Chem. Soc.*, 2017, **139**, 4330-4333.
- 14 23. J. Zhao, L. Xu, Y. Liu, Z. Yu, C. Li, Y. Wang and Z. Liu, *J. Phys. Chem. C*, 2015, **119**, 27657-
- 15 27665.
- 16 24. Q. Zhang, C. Chen, N. Li, Q. Huang, Y. He, X. Liu, B. Wang, D. Zhang, D. Y. Kim, Y. Wang, B.
- 17 Xu and W. Yang, *J. Phys. Chem. C*, 2018, **122**, 15929-15936.
- 18 25. J. Ketterer and V. Krämer, *Mater. Res. Bull.*, 1985, **20**, 1031-1036.
- 19 26. D. O. Charkin, P. S. Berdonosov, V. A. Dolgikh and P. Lightfoot, *J. Solid State Chem.*, 2003, **175**,
- 20 316-321.
- 21 27. Y. Yu, S. Huang, Y. Gu, S. Yan, Z. Lan, W. Zheng and Y. Cao, *Appl. Surf. Sci.*, 2018, **428**, 844-
- 22 850.
- 23 28. D. Zhang, P. K. Dera, P. J. Eng, J. E. Stubbs, J. S. Zhang, V. B. Prakapenka and M. L. Rivers, *J.*
- 24 *Vis. Exp.*, 2017, DOI: 10.3791/54660, 54660.
- 25 29. C. Prescher and V. B. Prakapenka, *High Pressure Res.*, 2015, **35**, 223-230.
- 26 30. A. C. Larson and R. B. Von Dreele, *Los Alamos National Laboratory, Los Alamos, NM*, 1986.

- 1 31. L. J. v. d. PAUW, *Philips Res. Rep.*, 1958, **13**, 1-9.
- 2 32. G. Zhang, Q. Zhang, Q. Hu, B. Wang and W. Yang, *J. Mater. Chem. A*, 2019, **7**, 4019-4025.
- 3 33. A. L. J. Pereira, D. Santamaría-Pérez, J. Ruiz-Fuertes, F. J. Manjón, V. P. Cuenca-Gotor, R.
- 4 Vilaplana, O. Gomis, C. Popescu, A. Muñoz, P. Rodríguez-Hernández, A. Segura, L. Gracia, A. Beltrán,
- 5 P. Ruleova, C. Drasar and J. A. Sans, *J. Phys. Chem. C*, 2018, **122**, 8853-8867.
- 6 34. V. S. Bhadram, L. Krishna, E. S. Toberer, R. Hrubciak, E. Greenberg, V. B. Prakapenka and T. A.
- 7 Strobel, *Appl. Phys. Lett.*, 2017, **110**, 182106.
- 8 35. X. Lü, W. Yang, Q. Jia and H. Xu, *Chem. Sci.*, 2017, **8**, 6764-6776.
- 9 36. J. Zhao, L. Wang, D. Dong, Z. Liu, H. Liu, G. Chen, D. Wu, J. Luo, N. Wang, Y. Yu, C. Jin and
- 10 Q. Guo, *J. Am. Chem. Soc.*, 2008, **130**, 13828-13829.
- 11 37. W. O. Uhoya, G. M. Tsoi, Y. K. Vohra, M. A. McGuire and A. S. Sefat, *J. Phys.: Condens. Matter*,
- 12 2011, **23**, 365703.
- 13 38. F. Birch, *Phys. Rev.*, 1947, **71**, 809-824.
- 14 39. D. Kato, K. Hongo, R. Maezono, M. Higashi, H. Kunioku, M. Yabuuchi, H. Suzuki, H. Okajima,
- 15 C. Zhong, K. Nakano, R. Abe and H. Kageyama, *J. Am. Chem. Soc.*, 2017, **139**, 18725-18731.
- 16 40. D. J. Payne, R. G. Egdell, A. Walsh, G. W. Watson, J. Guo, P. A. Glans, T. Learmonth and K. E.
- 17 Smith, *Phys. Rev. Lett.*, 2006, **96**, 157403.
- 18 41. A. Walsh, D. J. Payne, R. G. Egdell and G. W. Watson, *Chem. Soc. Rev.*, 2011, **40**, 4455-4463.
- 19 42. J. G. Cheng, K. E. Kweon, S. A. Larregola, Y. Ding, Y. Shirako, L. G. Marshall, Z.-Y. L. f, X.Li.,
- 20 António M. dos Santos, M. R. Suchomel, K. Matsubayashi, Y. Uwatoko, G. S. Hwang, John B.
- 21 Goodenough and J.-S. Zhou, *PNAS*, 2015, **112**, 1670-1674.
- 22 43. G. Liu, L. Kong, P. Guo, C. C. Stoumpos, Q. Hu, Z. Liu, Z. Cai, D. J. Gosztola, H.-k. Mao, M. G.
- 23 Kanatzidis and R. D. Schaller, *ACS Energy Lett.*, 2017, **2**, 2518-2524.
- 24